Hindawi
International Journal of Energy Research
Volume 2024, Article ID 4589047, 15 pages
https://doi.org/10.1155/2024/4589047

WILEY | Hindawi

Research Article

Enhanced Photocatalytic and Electrochemical Performance of MOF-Derived NiO-ZnO Oxide Composites for Wastewater Treatment and Sustainable Energy Storage

S. V. Prabhakar Vattikuti,[1] **Jaesool Shim**,[1] **Nam Nguyen Dang**,[2,3] **P. Rosaiah**,[4] **Mohammad Rezaul Karim**,[5] **Ibrahim A. Alnaser**,[5] **and Baseem Khan**[6]

[1]*School of Mechanical Engineering, Yeungnam University, Gyeongsan 38541, Republic of Korea*
[2]*Faculty of Civil Engineering, Duy Tan University, Danang 550000, Vietnam*
[3]*Future Materials & Devices Lab., Institute of Fundamental and Applied Sciences, Duy Tan University, Ho Chi Minh City 700000, Vietnam*
[4]*Department of Physics, Saveetha School of Engineering, Saveetha Institute of Medical and Technical Sciences, Chennai 602105, India*
[5]*Department of Mechanical Engineering, College of Engineering, King Saud University, Riyadh 11421, Saudi Arabia*
[6]*Department of Electrical and Computer Engineering, Hawassa University, Hawassa 05, Ethiopia*

Correspondence should be addressed to Jaesool Shim; jshim@ynu.ac.kr, Nam Nguyen Dang; nguyendangnam@duytan.edu.vn, and Baseem Khan; basseemk@hu.edu.et

Received 11 October 2023; Revised 13 February 2024; Accepted 29 February 2024; Published 1 April 2024

Academic Editor: Vinayak Parale

Solar energy is a crucial and sustainable resource, necessitating material optimization for efficient use in solar-driven applications, particularly photocatalysis. Mixed-metallic nanocomposites, notably those derived from metal-organic frameworks (MOFs), have emerged as promising functional materials for environmental remediation and electrochemical energy storage. MOFs provide unique platforms for synthesizing diverse nanostructures, incorporating metals, oxides, sulfides, and nitrides within a porous carbon matrix. These resulting nanocomposites exhibit high crystallinity, retained morphologies, and tunable textural features. This study focuses on synthesizing a MOF-derived Ni/Zn nanocomposite (i.e., MD-Ni/Zn) from a bimetallic MOF to exploit its potential in photocatalytic pollutant degradation and electrochemical energy storage. Under UV irradiation, the MD-Ni/Zn nanocomposite efficiently degrades 98% of mixed (RhB + CV) dye within 60 minutes. This remarkable photocatalytic performance is attributed to the occurrence of mixed phases in the MD-Ni/Zn nanocomposite, minimizing the recombination efficiency of photoinduced e^-/h^+ through the p-n heterojunction mechanism. Electrochemical analysis reveals outstanding capacitance in the MD-Ni/Zn nanocomposite, reaching 1002 F/g at 5 A/g, emphasizing its suitability for enhanced electrochemical energy storage.

1. Introduction

The environment faces an unprecedented crisis, wrought by the relentless impact of human activities compounded by the relentless march of industrialization. This relentless industrialization, coupled with an excessive reliance on fossil fuels to satiate our insatiable energy needs, casts a dark shadow over our future. Researchers worldwide have recognized the urgent need to address this looming environmental catastrophe, making environmental remediation and energy crisis mitigation paramount global priorities [1]. The salvation of our ecosystem demands concerted and sustainable efforts. In this quest for environmental preservation, photocatalytic degradation has emerged as a powerful, economical, and widely embraced approach for treating contaminated wastewater. Its appeal lies in its remarkable capacity to transform

toxic organic dyes into environmentally benign compounds, including carbon dioxide and other carbonaceous products. Recent scientific investigations have shed light on a promising avenue for enhancing this process—the development of nanocomposite materials possessing band gap energies compatible with solar light and a propensity for minimizing the recombination of photoinduced electron-hole pairs [2–7]. For instance, Paul et al. [8] reported the impressive UV light-driven MB dye degradation efficiency of 74.87% achieved by a NiO-ZnO composite within 120 minutes of irradiation. Similarly, Far et al. [9] demonstrated that a NiO/Fe_2O_3/PVA composite achieved nearly 100% efficiency in MB dye degradation within just 90 minutes, attributed to the synergistic effects of mixed metal oxides. These findings underscore the promise of nanocomposite materials in advancing the effective removal of synthetic dyes through photocatalysis, marking a significant stride in our efforts to address the environmental challenges at hand.

The exponential expansion of advanced technologies and industrial sectors has precipitated a relentless pursuit of alternative green energy solutions, driven by the imperative to address energy storage and conversion challenges [10]. In this context, supercapacitors have emerged as a pivotal contender, offering the potential to bridge the energy and power gap and thereby presenting a promising avenue for green energy production. Their applications span diverse domains, including transportation, portable electronic devices, and smart grid systems. However, despite their numerous advantages, the intrinsic limitation of low energy density has thus far prevented supercapacitors from fully supplanting traditional batteries in the market [10, 11]. Consequently, significant research endeavors are currently underway to engineer flexible and lightweight electrodes for hybrid supercapacitors, amalgamating capacitive and battery-like characteristics, with the overarching aim of enhancing device performance and commercial viability.

MOFs, renowned for their porous nature, have garnered substantial attention across the disciplines of physics, chemistry, biology, and material science [12–15]. These crystalline porous materials boast a well-defined interrupted network construction, made through the self-association and building of inorganic metal centers and organic ligands. MOFs offer a host of advantages, including high functionality, substantial surface area, precise pore dimension control, and exceptional porosity. Their tunable features and myriad metal/ligand conformations render them invaluable in applications spanning adsorption, catalysis, and electrochemical energy storage. MOFs offer easily tailored surface properties and well-ordered pore structures, serving as ideal precursors for versatile porous carbon materials. Notably, mixed metal-MOFs have emerged through the simultaneous incorporation of mixed metal species with organic ligands [16, 17]. These materials offer distinct advantages over conventional templates, primarily due to the molecular-level mixing of metal species within MOFs, the ability to maintain homogeneous morphologies, and enhanced structural integrity that minimizes undesired aggregation or framework collapse during thermolysis [18, 19].

Recent research demonstrates the efficient conversion of MOFs into metal oxide/porous carbon composites through inert atmosphere pyrolysis. This process leverages the regular coordination bonds formed between metal ions and organic ligands within MOF crystals, facilitating the uniform and orderly dispersion of metal/metal oxides within the resulting composite carbon materials. As a result, nanocomposites derived from MOFs are acknowledged as potent adsorbents for purging wastewater pollutant. For example, Jin et al. [20] reported the successful preparation of MOF-derived Ni/porous carbon-CNT composite via carbonization, exhibiting a maximum RhB dye absorption capacity of 395 mg/g, with the added benefit of regenerability through ethanol washing. Likewise, Li et al. [21] demonstrated that a Co_3O_4-Bi_2O_3 composite exhibited remarkable peroxymonosulfate activation activity, leading to nearly 100% degradation of RhB within just 30 minutes, attributed to the enhancing influence of bi species on the activation capacity of Co_3O_4 within the composite. Additionally, Wang et al. [22] reported the synthesis of an MOF-derived C-doped ZnO/TiO_2 composite, which exhibited exceptional photocatalytic degradation efficiency, achieving a 94% degradation of RhB under simulated solar light irradiation. These findings collectively underscore the remarkable potential of MOF-derived nanocomposites in advancing diverse environmental and energy-related applications, marking a significant stride in our quest to address pressing challenges.

Recent advancements in materials science have revealed the potential for enhancing the photocatalytic activity of mixed metal oxide composite photocatalysts by constructing heterojunctions between NiO and other metal oxides with appropriately aligned band positions or doping approach [23–25]. The creation of p-n junctions and the establishment of an internal built-in electric field have been recognized as highly effective strategies for promoting the efficient separation of photoinduced charge carriers [26, 27]. Li et al. [28] reported that the p-n heterojunction designed in the NiO-CeO_2 nanocomposite significantly enhanced the removal efficiency of MO dye under UV irradiation, resulting in a 2.6-fold improvement compared to bare NiO. This enhancement was endorsed to the favorable features of p-n heterojunctions for efficient charge separation and rapid transfer of electron-hole pairs. Furthermore, MOF-derived materials have proven instrumental in addressing environmental issues, particularly in the realm of photocatalytic pollutant degradation. Lei et al. [29] demonstrated that an MOF-derived hollow CuO/ZnO composite achieved an impressive 87% degradation of tetracycline hydrochloride under visible light irradiation within 60 minutes.

Beyond their environmental applications, MOF-derived metal oxides have also shown great promise in the field of electrochemical energy storage [30]. Supercapacitors, known for extended cycling, high power, ecofriendliness, safety, and conductivity, are vital energy stores. Pseudocapacitors, in particular, leverage the reversible redox reactions of metal oxides or sulfides to deliver impressive energy storage capacities. Mixed metal-metal oxide-based electrodes, which capitalize on the synergy of mixed metal species to enhance electrical conductivity and surface area compared to

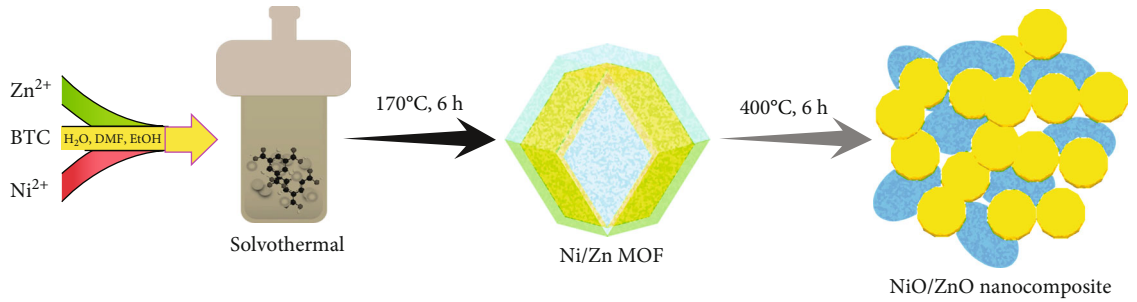

Figure 1: Schematic representation of synthetic procedure of the MD-Ni/Zn composite.

monometallic oxides, have become a common choice for supercapacitor electrode preparation. These electrodes facilitate increased charge pathways for energy storage. For instance, Yang et al. [31] developed a $NiCo_2O_4$/NiO composite derived from the pyrolysis of Ni/Co-MOF, achieving a remarkable electrochemical storage capability of 726 F/g at 1 A/g, with remarkable working stability, retaining 91.4% of its capacity over 5000 cycles. Aghazadeh and Foratirad [32] reported that a $Ni_{2-x}Zn_x$ $(OH)_2$@C electrode demonstrated impressive capacities of 545 mAh/g at 5 A/g, with 91.8% retention over 6000 cycles. Tang et al. [33] reported Ni/ZnO nanosponges from MOF derivatives with 807 F/g capacitance at 1 A/g and 86% retention over 5000 cycles.

In this study, we present the synthesis and characterization of a bimetallic MOF-derived Ni/Zn (MD-Ni/Zn) composite via pyrolysis in an air environment. We explore the photocatalytic efficiency of the MD-Ni/Zn composite by evaluating its performance in degrading mixed (RhB + CV) dye in aqueous solutions. Furthermore, our investigation reveals remarkable electrochemical activity, with the MD-Ni/Zn composite exhibiting a capacitance of 1002 F/g at 5 A/g. These findings underscore the mixed faceted potential of MOF-derived materials in addressing critical environmental and energy-related challenges.

2. Experimental Details

Nickel (II) nitrate hexahydrate and zinc nitrate hexahydrate from Daejung, trimesic acid (BTC) from Sigma-Aldrich, and N,N-dimethylformamide (DMF) from Alfa Aesar are used as received. The preparation procedure of the Ni-MF, Zn-MF, and Ni/Zn-MF was discussed in reported literature [10] with slight modifications. In details, equal volumes of DI water, DMF, and ethanol solutions (totaling 210 mL) are prepared. Each of 137 mg of $Ni(NO_3)_2.6H_2O$ and $Zn(NO_3)_2.6H_2O$ are added to 80 mL of above stock solution, stirred at 200 rpm for 10 min, and then added dropwise of 103 mg of BTC in 130 mL solution. The resulting mixture is transferred to a Teflon autoclave reactor and kept at 170°C for 6 h. Finally, the precipitate is separated via centrifugation at 8000 rpm, washed repeatedly with methanol, and kept at 100°C for 10 h. To synthesize Ni-MF and Zn-MF, we repeat the procedure without the Ni or Zn precursor. To obtain the NiO, ZnO, and NiO/ZnO composites, the materials obtained above are subjected to calcination at 400°C for 6 h, resulting in MOF-derived NiO (i.e., MD-NiO), MOF-derived ZnO (i.e., MD-ZnO), and MD-Ni/Zn composites (Figure 1).

The materials' structural and crystalline properties were examined through XRD (XRD-6100, Shimadzu, Japan) with CuKα radiation. Surface morphology and microstructure analyses were conducted using SEM, Hitachi, S-4100 and HRTEM, Tecnai G2 F20 S-Twin at an acceleration voltage of 200 kV. The elemental composition on the sample surface was determined by HRTEM-EDS. Additionally, the chemical states of the materials were analyzed using Thermo Scientific XPS with Al Kα radiation.

The photocatalytic performance of all catalysts was evaluated by simulating the decolorization of a mixed dye solution (RhB + CV, 1 : 1) under UV light irradiation. Specifically, 50 mg of each sample was mixed in 100 mL of the RhB + CV aqueous solution. Prior to irradiation, the solution was left in the dark for 30 min. Subsequently, UV light was applied. At specified time intervals, 5 mL of the solution was extracted, and the sample was separated by centrifugation. Spectral measurements were conducted on the supernatant after centrifugation using a UV-Vis spectrophotometer (Neo-D3117, Neogen).

The electrochemical performance of the samples was evaluated using a conventional three-electrode cell. A saturated Hg/HgO reference electrode and a platinum mesh counter electrode were employed. The working electrode was prepared as a slurry by combining active materials, carbon black, and PVDF in a mass ratio of 90 : 5 : 5 in NMP. The slurry mixture was then drop-cast onto Ni foam and dried in an oven at 80°C for 2 h. CV tests were conducted at various scan rates within a potential window of 0.0 V to 0.6 V. GCD tests were carried out in the range of 0–0.5 V vs the Hg/HgO reference electrode at altered current densities. EIS measurements were performed over a frequency range of 200 kHz to 100 Hz. All electrochemical experiments were conducted in a 1.0 M KOH using a Biologic SP-200 electrochemical system.

3. Results and Discussion

XRD profiles of all the samples (Figure 2) exhibit a high degree of compatibility with one another, and the sharpness of the respective peaks serves as evidence of the inherent

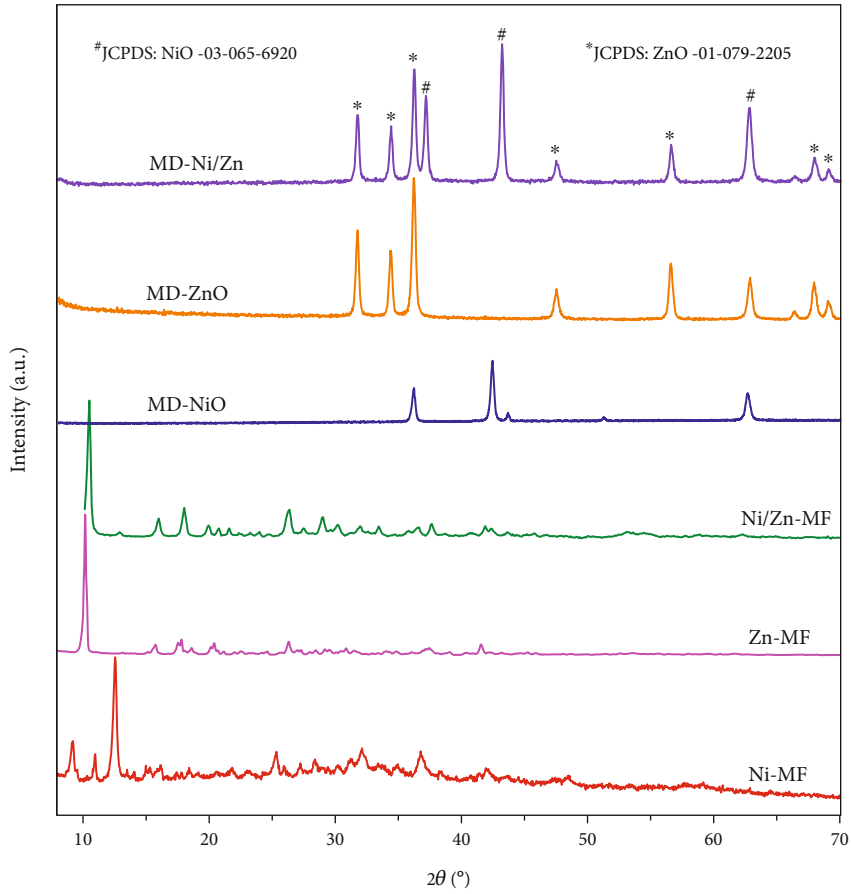

Figure 2: XRD patterns of Ni-MF, Zn-MF, Ni/Zn-MF, MD-NiO, MD-ZnO, and MD-Ni/Zn composite.

crystallinity of these materials. In the case of the Ni-MF sample, a prominent peak at 12.4° corresponds to the (110) plane of Ni-MOF [34]. In contrast, the Zn-MF and Ni/Zn-MF samples display three major peaks located at 12.56°, 33.35°, and 59.27°, which align well with the reported literature [35–37]. Furthermore, the XRD pattern of Ni/Zn-MF aligns consistently with that of Zn-MF samples, featuring a characteristic peak of Zinc MOF at 10.5° [38]. It is worth noting that the MOF structures can vary under different synthesis conditions. After undergoing oxidizing calcination at 400°C, both the Ni-MF and Zn-MF samples exhibit XRD patterns that closely match those of pure NiO (JCPDS no: 03-65-6920) and ZnO (JCPDS no: 01-079-2205). This alignment signifies the complete removal of organic ligands from the MOF samples and the conversion of Ni/Zn species into oxide phases. However, it is worth noting that in the Ni/Zn composite, there is a reduction in the intensity of the diffraction peaks, which can be attributed to lattice distortion [39]. In contrast, in the Ni/Zn-MF sample, distinct peaks corresponding to NiO and ZnO phases are observed in the oxidized sample, resulting in the formation of the NiO-ZnO composite.

The photocatalytic and electrochemical activities of nanomaterials are well-established to be closely correlated with their morphology, particle size, and the presence of active sites. The morphologies of MOF materials undergo significant changes during the calcination process, primarily due to the removal of guest molecules and the decomposition of organic components as a result of the heat treatment process. As depicted in Figures 3(a) and 3(b), the FESEM images of MD-NiO reveal a distinctive structure resembling clustered pocky sticks, composed of agglomerated NiO and ZnO nanoparticles. Conversely, MD-ZnO (Figures 3(c) and 3(d)) displays relatively agglomerated particles that are dispersed in a random order. Notably, the MD-Ni/Zn composite, as illustrated in Figures 3(e)–3(h), showcases a distinct egg-yolk-like structure composed of mixed oxide materials. In comparison to MD-NiO, a notable porous structure is evident on the surface of MD-Ni/Zn, suggesting that the ZnO particles are uniformly distributed and loaded onto the surface, achieving the desired egg-yolk-like configuration. This highly dispersed surface structure is of paramount significance as it leads to an increased abundance of active sites and expanded surface area. Furthermore, the synergy effect ascending from the combination of mixed metal oxides within the composite further amplifies its suitability for catalytic applications. This synergy arises from the unique interplay of mixed metal oxides, resulting in enhanced catalytic performance beyond what would be achievable with individual components alone. The egg-yolk-like architecture, along with the synergistic effects, establishes the MD-Ni/Zn composite as a promising candidate for various catalytic applications, owing to its exceptional surface characteristics and catalytic potential.

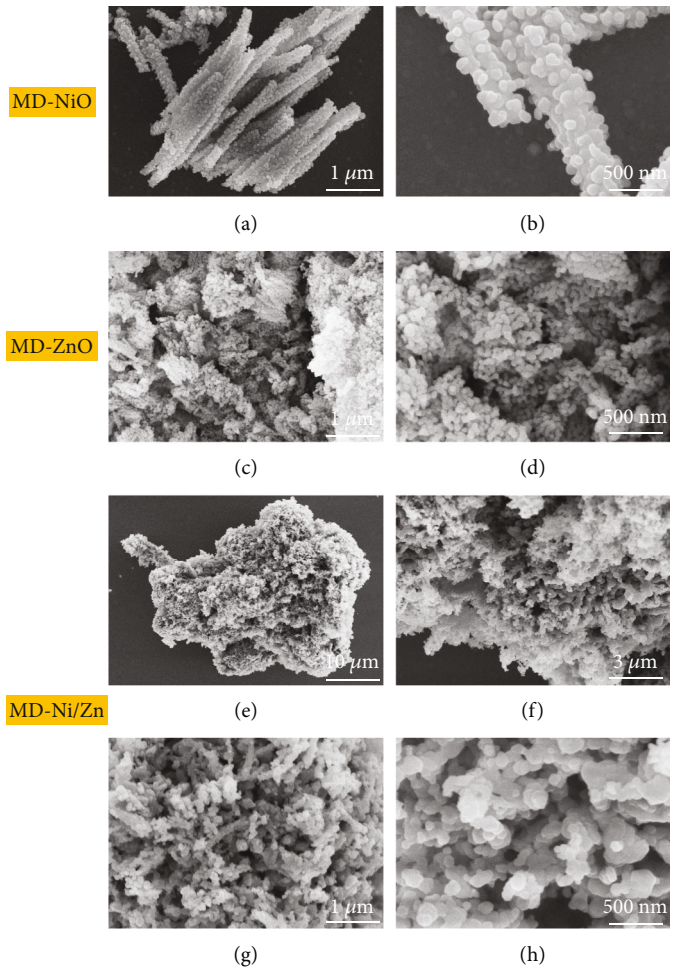

Figure 3: FESEM images (a, b) MD-NiO, (c, d) MD-ZnO, and (e–h) MD-Ni/Zn composite.

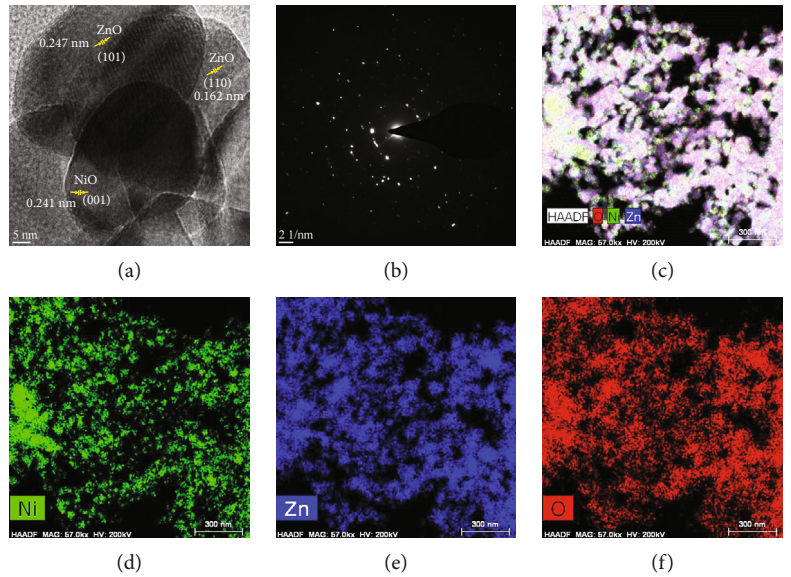

Figure 4: (a) HRTEM images, (b) SEAD pattern, (c) combined elemental mapping, and (d–f) individual elemental mapping of MD-Ni/Zn composite.

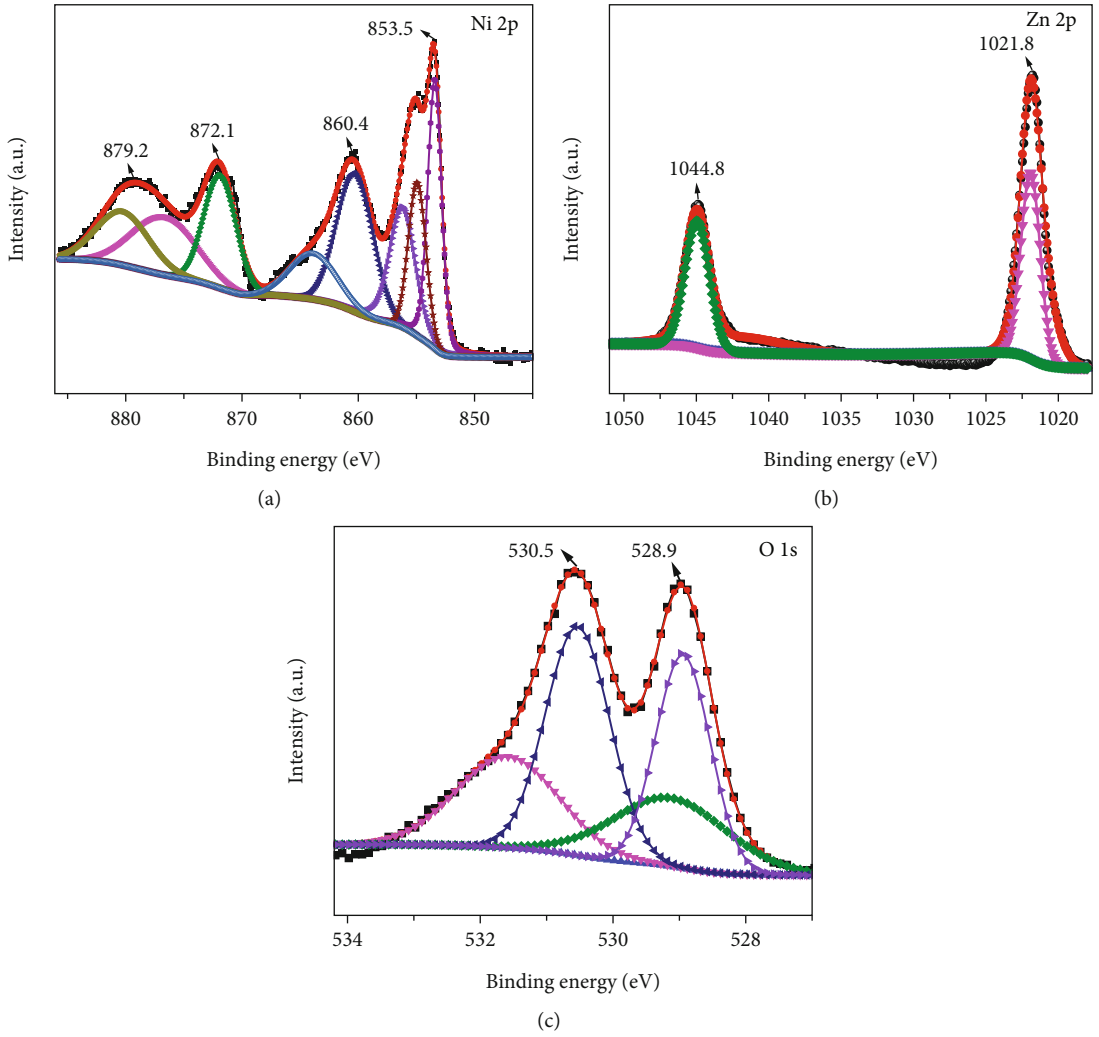

Figure 5: XPS spectra of MD-Ni/Zn composite (a) Ni 2p, (b) Zn 2p, and (c) O 1s spectra.

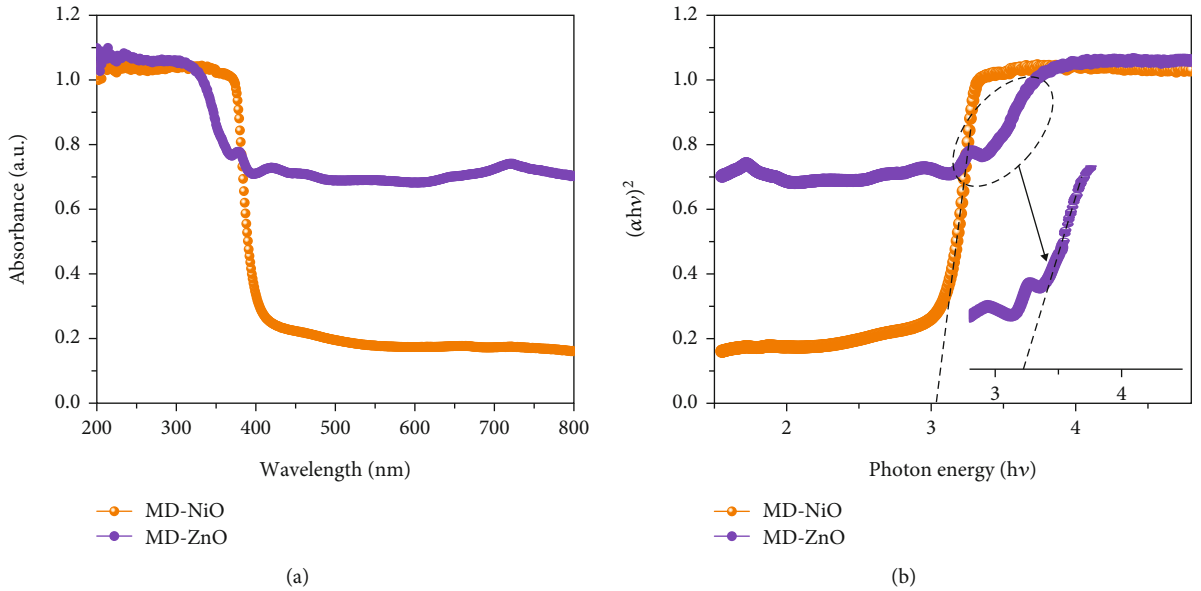

Figure 6: (a) Optical absorbance spectra and (b) Tauc plots of MD-NiO, MD-ZnO, and MD-Ni/Zn composite.

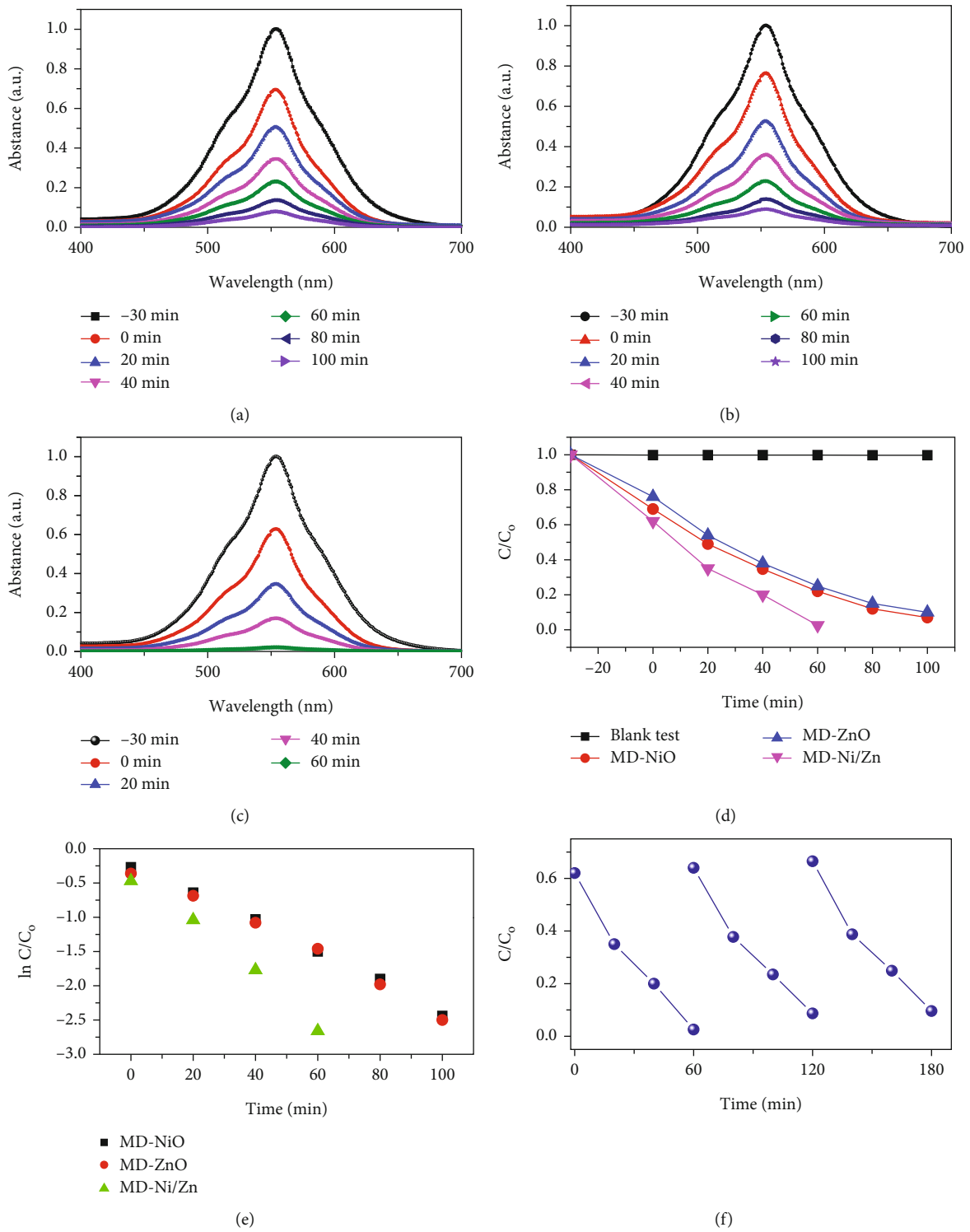

Figure 7: UV-Vis absorption spectra of mixed (RhB + CV) dye degradation utilizing (a) MD-NiO, (b) MD-ZnO, and (c) MD-Ni/Zn composite under UV irradiation; (d) photocatalytic activity assessment and (e) kinetic curves for MD-NiO and MD-Ni/Zn composite; and (f) stability test results for MD-Ni/Zn composite.

Figure S1 (a, b) and Figure 4 present HRTEM images of the MD-Ni/Zn composite. In Figure 4(a), the MD-Ni/Zn composite exhibits an egg-yolk-like structure composed of aggregated nanoparticles. The lattice stripes of ZnO (101, 0.247 nm) and (110, 0.162 nm), as well as NiO (001, 0.241 nm) planes with their respective lattice spacings, are clearly distinguishable. These images provide a detailed view of the composite's internal structure, highlighting the presence of well-defined boundaries between the core and shell components. Figure 4(b) displays a SAED pattern,

characterized by ring and dot patterns. This pattern serves as clear evidence of the coexistence of mixed metal oxides within the composite, further confirming its mixed-metallic nature. Figure 4(c) exhibits combined elemental mapping of the MD-Ni/Zn composite. These images unequivocally validate the purity of the sample, showcasing a homogenous distribution of constituent elements. To further corroborate this, individual elemental mapping of Ni, Zn, and O elements is depicted (Figures 4(d)–4(f)), and as observed, these elements are homogeneously dispersed in the composite. Additionally, EDX spectra of the MD-Ni/Zn composite (Figure S1c) provide quantitative information about the elemental composition. These spectra align with the elemental mapping results, further confirming the presence and even distribution of Ni, Zn, and O elements within the composite. Collectively, these characterizations underscore the structural integrity, purity, and mixed-metallic nature of the MD-Ni/Zn composite, establishing its suitability for various applications. The formation mechanism of the MOF-derived NiO-ZnO oxide composites can be elucidated through the following sequential processes: (i) Initially, protons generated through the hydrolysis of Zn^{2+} ions readily interact with Ni^{2+} ions, leading to the liberation of bimetallic ions; (ii) concurrently, a portion of the liberated Ni^{2+} ions undergo oxidation, transitioning into Ni^{3+} ions due to the presence of dissolved O_2 and NO_3^- in the solution. These Ni^{3+} ions then coprecipitate with Zn^{2+} ions, resulting in the formation of the composite, wherein they become integrated with the BTC ligands, and (iii) furthermore, during the subsequent calcination process, the guest molecules that serve as linkers within the MOF structure vaporize. This vaporization process contributes to the formation of the NiO-ZnO matrix. This multistep process underscores the intricate yet controlled formation of the NiO-ZnO oxide composites, with each step playing a crucial role in shaping the final composite structure.

Figure 5 illustrates the XPS spectrum of the MD-Ni/Zn composite, providing valuable insights into its elemental composition and chemical states. In the Ni 2p XPS profile (Figure 5(a)), two distinct component peaks are evident, corresponding to the Ni $2p_{3/2}$ (853.5 eV) and Ni $2p_{1/2}$ (872.1 eV) spin-orbit planes of NiO. These peaks unequivocally confirm the presence of Ni^{2+} states within the composite. Furthermore, the characteristic satellite features of Ni^{3+} are also observed at 860.4 and 879.2 eV [40], offering additional evidence of the coexistence of Ni^{3+} ions. From Figure 5(b), the Zn 2p XPS spectrum reveals two distinct peaks positioned at 1021.8 eV and 1044.8 eV, which can be endorsed to Zn $2P_{3/2}$ and Zn $2p_{1/2}$, respectively. These findings approve the presence of Zn^{2+} states within the composite [41]. Lastly, in Figure 5(c), the O1s XPS profile of the MD-Ni/Zn composite is presented, revealing a well-resolved spectrum comprising distinct peaks at 528.9 and 530.5 eV; these findings align with prior literature reports [42]. Overall, the XPS analysis provides comprehensive evidence regarding the chemical states and elemental composition of the MD-Ni/Zn composite, further supporting its suitability for various applications.

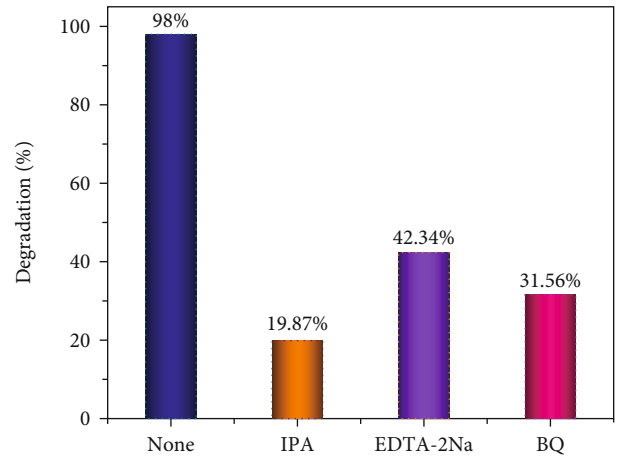

Figure 8: Trapping test results over different scavengers.

Figure 6(a) presents the UV-Vis-NIR absorption spectra of MD-NiO and MD-ZnO samples, revealing high UV absorption characteristics. Additionally, Figure S2 presents a comparison of the optical performance between MD-NiO, MD-ZnO, and MD-Ni/Zn composite materials. The prominent absorption peaks are endorsed to the respective band gaps of these samples. However, when comparing MD-NiO to MD-ZnO, it is apparent that MD-ZnO exhibits weaker absorption, suggesting an impact of large size of nanoparticle on the optical characteristics of MD-ZnO. This effect is corroborated by high-magnification HRTEM images (Figure 4). Figure 6(b) shows plots of $(\alpha h\nu)^2$ vs $h\nu$, yielding band gap (E_g) values of approximately 2.98 eV and 3.21 eV for MD-NiO and MD-ZnO samples, respectively. On the other hand, the MD-Ni/Zn composite exhibited a band gap of 3.14 eV (Figure S2).

To assess the photocatalytic properties of the composite, the photodegradation of mixed (RhB + CV) dyes was studied, with a 30-minute dark absorption period to reach adsorption-desorption equilibrium. UV-Vis absorption spectra were recorded over varying irradiation times, as depicted in Figures 7(a)–7(c). Figure 7(d) shows the photocatalytic activity over the MD-NiO and MD-Ni/Zn composite of the mixed dye degradation under UV irradiation. A blank test of mixed (RhB + CV) dyes revealed no significant removal, indicating the absence of photodegradation without a photocatalyst. Under UV light irradiation, the photocatalytic degradation rates of mixed (RhB + CV) dyes over MD-NiO and MD-Ni/Zn reached 99% and 98% within 100 minutes and 60 minutes, respectively. These results highlight the significantly enhanced photocatalytic capacity of MD-Ni/Zn composite compared to MD-NiO. This improvement is endorsed to the mixed metal interface effect within the MD-Ni/Zn composite. Furthermore, the apparent reaction rate constant (k) was estimated using the equation $\ln(C/C_o) = kt$, where C and C_o refer to the initial and operating time (t) concentrations of the mixed dye, and k is the rate constant. Figure 7(e) reveals that the degradation of the mixed dye follows a pseudo-first-order kinetic characteristic. The estimated k values for MD-NiO and MD-Ni/Zn composite are 0.021 and 0.038 min^{-1}, respectively. The shorter reaction time observed

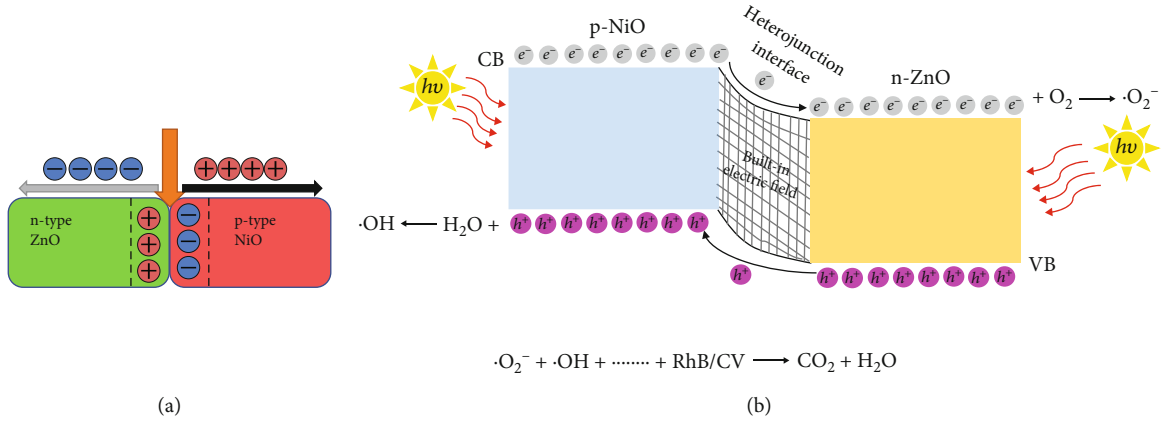

Figure 9: (a, b) Proposed photocatalytic mechanism of MD-Ni/Zn composite.

for the MD-Ni/Zn composite is endorsed to the p-n heterojunction features, facilitating rapid charge transfer and improved separation efficiency during the photocatalytic process, ultimately enhancing the photoactivity of the MD-Ni/Zn composite [43]. Figure 7(f) presents the working stability of the MD-Ni/Zn composite during three recycling runs for mixed dye removal. These results demonstrate negligible changes in the degradation of mixed dye, underscoring the robust and stable performance of the MD-Ni/Zn composite over multiple cycles.

We utilized various scavengers (IPA, BQ, and EDTA-2Na) to probe the roles of ·OH, O_2^-, and h^+ radicals (Figure 8). The addition of scavengers led to a significant reduction in the degradation rates of mixed dye, dropping from 98% to 31.56%, 19.87%, and 42.34% in the attendance of BQ, IPA, and EDTA-2Na, respectively. This observation indicates that ·OH is the primary reactive species, while $\cdot O_2^-$ and h^+ radicals also play important roles in mixed dye degradation. The reaction can be approximately characterized by the following equations:

$$\begin{aligned}
\mathrm{NiO} &\longrightarrow \mathrm{NiO}\left(e^- + h^+\right),\\
\mathrm{ZnO} &\longrightarrow \mathrm{ZnO}\left(e^- + h^+\right),\\
\mathrm{NiO}\left(e^-\right) + O_2 &\longrightarrow \mathrm{NiO} + \cdot O_2^-,\\
\mathrm{ZnO}\left(e^-\right) + O_2 &\longrightarrow \mathrm{ZnO} + \cdot O_2^-,\\
\mathrm{NiO}\left(h^+\right) + H_2O &\longrightarrow \mathrm{NiO} + \cdot OH + h^+,\\
\mathrm{ZnO}\left(h^+\right) + H_2O &\longrightarrow \mathrm{ZnO} + \cdot OH + h^+,\\
(\mathrm{RhB} + \mathrm{CV}) + \left\{\cdot O_2^-, h^+, \cdot OH\right\} &\longrightarrow CO_2 + H_2O + \text{other products}.
\end{aligned} \tag{1}$$

Taking into account the experimental results and relevant literature, the photocatalytic mechanism of the NiO/ZnO composite is schematically represented in Figure 9. When bimetallic Ni/Zn MOF undergoes calcination, it forms a p-n heterojunction between p-NiO and n-ZnO, establishing a built-in electric field at the interface. This electric field induces a negative charge in the p-NiO region and a positive charge in the n-ZnO region for charge equilibrium (Figure 9(a)). Under UV irradiation (Figure 9(b)), electrons become excited, moving from the VB to the CB in NiO and then to the CB of ZnO due to the built-in electric field. Concurrently, holes migrate from the VB of ZnO to the VB of NiO. The photoinduced electrons react with O_2 molecules adsorbed in the dye to form $\cdot O_2^-$ radicals [44]. Conversely, holes transported as of the VB of n-ZnO to that of p-NiO interact with the water in the dye to generate ·OH radicals [45]. Consequently, the recombination of photoinduced e^-/h^+ is significantly inhibited. The $\cdot O_2^-$ and ·OH radicals work in tandem to degrade the dye into nonpolluting products, including CO_2 and H_2O. Thus, the heterojunction between NiO and ZnO plays a pivotal role in suppressing the recombination of photoinduced e^-/h^+ pairs and enhancing the photocatalytic activity.

We conducted a comprehensive investigation into the electrochemical activity of MOF-derived samples, specifically MD-NiO and MD-Ni/Zn composites, and performed a comparative analysis. As depicted in Figures 10(a) and 10(b), the CV profiles of MD-NiO and MD-Ni/Zn composite electrodes were examined across a range from 1 to 20 mV/s. Analyzing the CV curves reveals that at low scan rates, the MD-Ni/Zn composite exhibits more prominent redox peaks compared to MD-NiO. Remarkably, the MD-Ni/Zn composite exhibits the largest integrated area in the CV profile, signifying superior specific capacitance and heightened redox activity. With increasing scan rates, both electrode types maintain distinct redox peaks. Furthermore, noticeable shifts in oxidation and reduction peaks suggest typical pseudocapacitive behavior [46]. In both cases, the electrodes display distinct redox peaks corresponding to the pseudocapacitance behavior of NiO and NiO/ZnO. The intensity of these peaks increases with higher scan rates, affirming that both electrode materials possess pseudocapacitance activity. Among them, the MD-Ni/Zn composite electrode exhibits the highest peak current, indicating enhanced electrochemical performance. The increased peak current observed in the MD-Ni/Zn composite electrode can be endorsed to the synergy effect resulting from the combination of NiO and ZnO within the composite electrode [47–49]. This enhanced electrochemical performance can be explained by considering the conceivable reaction

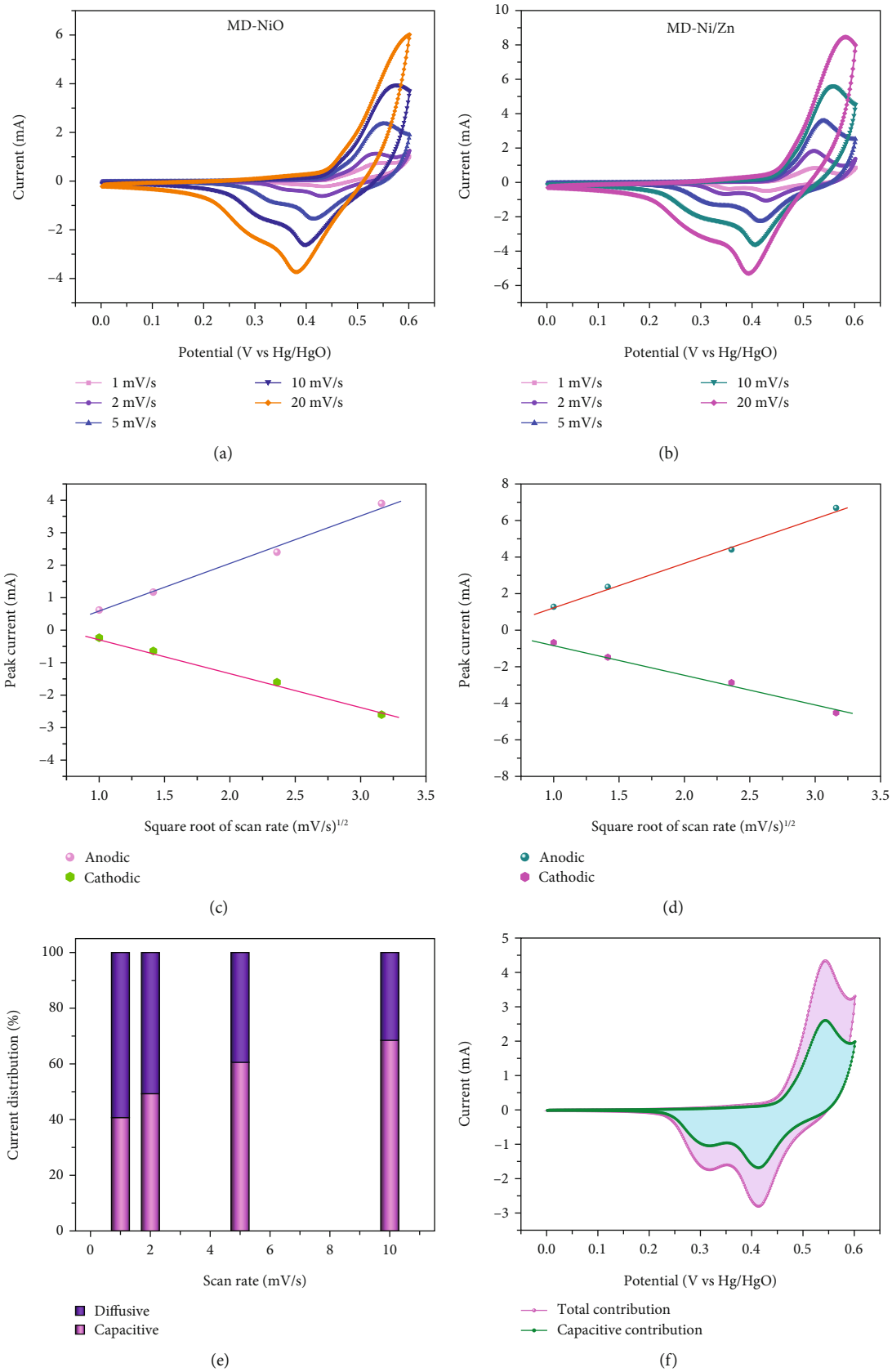

Figure 10: CV curves of (a) MD-NiO and (b) MD-Ni/Zn composite, anodic/cathodic peak current vs square root of scan rate of (c) MD-NiO and (d) MD-Ni/Zn composite, (e) detailed breakdown of capacitive and diffusive contributions, and (f) a comparative analysis of the total contribution and capacitive contribution for the MD-Ni/Zn composite electrode.

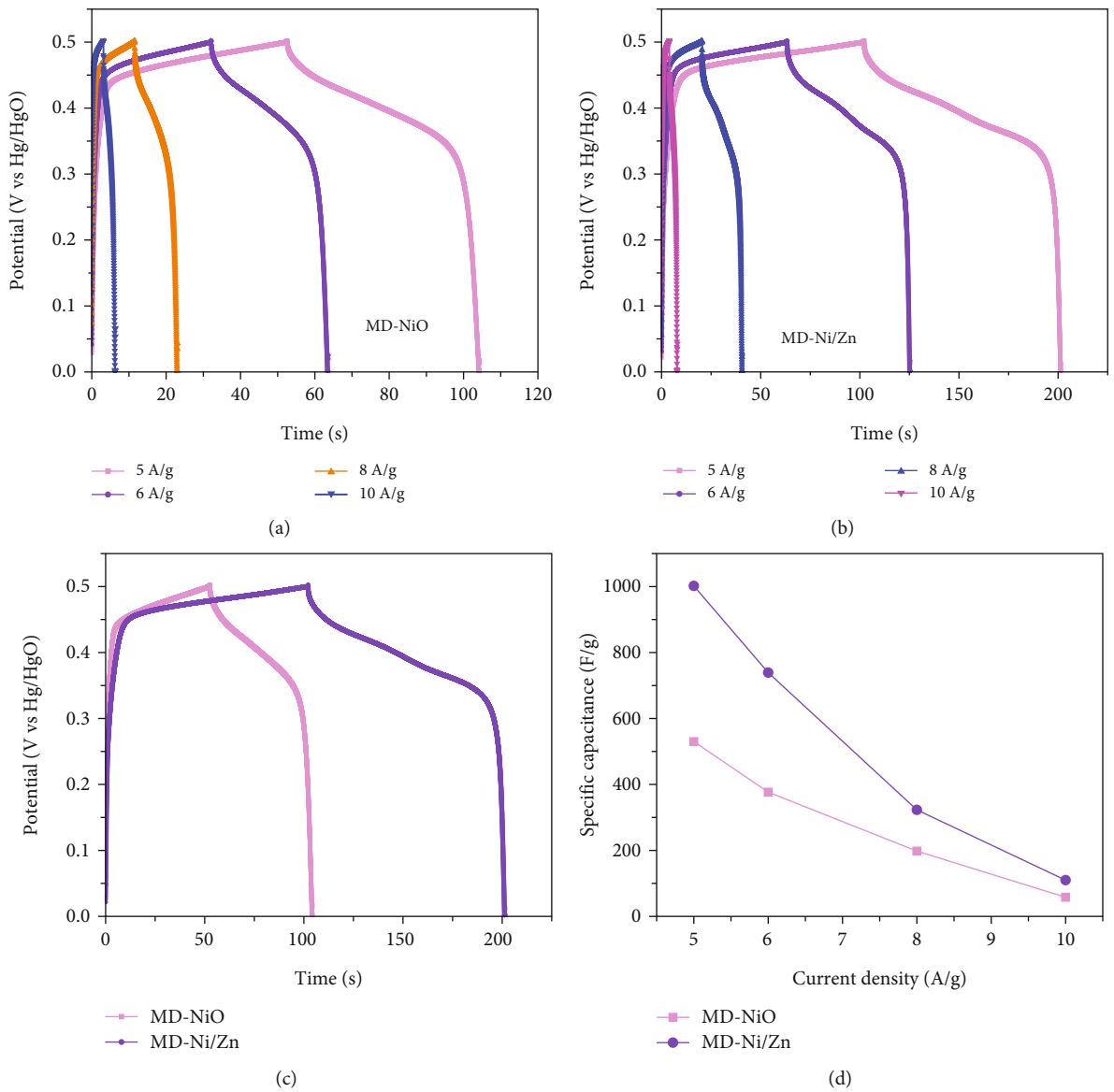

Figure 11: GCD profiles of (a) MD-NiO, (b) MD-Ni/Zn composite, (c) comparison of MD-NiO and MD-Ni/Zn composite electrodes, and (d) specific capacitance vs current density of MD-NiO and MD-Ni/Zn composite electrodes.

mechanisms associated with the intercalation/deintercalation of K^+ ions into the MD-Ni/Zn electrode. These reactions can be elucidated as follows:

$$\begin{aligned} \mathrm{MD}-\frac{\mathrm{Ni}}{\mathrm{Zn}}+\mathrm{K}^{+}+\mathrm{e}^{-} &\longleftrightarrow \left[\mathrm{K}-\mathrm{MD}-\frac{\mathrm{Ni}}{\mathrm{Zn}}\right]\text{surface}, \\ \mathrm{MD}-\frac{\mathrm{Ni}}{\mathrm{Zn}}+\mathrm{K}^{+}+\mathrm{e}^{-} &\longleftrightarrow \left[\mathrm{MD}-\frac{\mathrm{Ni}}{\mathrm{Zn}}\right]\mathrm{K}. \end{aligned} \tag{2}$$

These equations illustrate the adsorption of K^+ ions onto the surface of electrode and/or the intercalation/deintercalation of K^+ cations from the electrolyte at the MD-Ni/Zn composite and electrolyte interface. During the charging process, K^+ ions from the electrolyte insertion into the MD-Ni/Zn electrode surface. Conversely, through discharge, K^+ ions are removed from the MD-Ni/Zn composite and diffuse back into the aqueous media, completing the electrochemical cycle.

In Figures 10(c) and 10(d), the association between peak current and the square root of scan rates ranging from 1 to 20 mV/s is presented. For 1 to 20 mV/s, the peak current demonstrates a consistent increase, displaying a linear correlation with the square root of the scan rates. This behavior indicates that the kinetics of the electrode redox reaction are governed by the interplay between the surface-diffusion reaction of OH^- ions and the adsorption/desorption processes occurring on the electrode surface. Figure 10(e) illustrates the separation of surface-controlled and diffusion-controlled processes, revealing the capacitive and diffusive contributions of the MD-Ni/Zn composite electrode at different scan rates. It is perceived that the diffusive contribution becomes more prominent as the cumulative scan rate increases (1-10 mV/s). Specifically, the percentage of capacitive contribution gradually

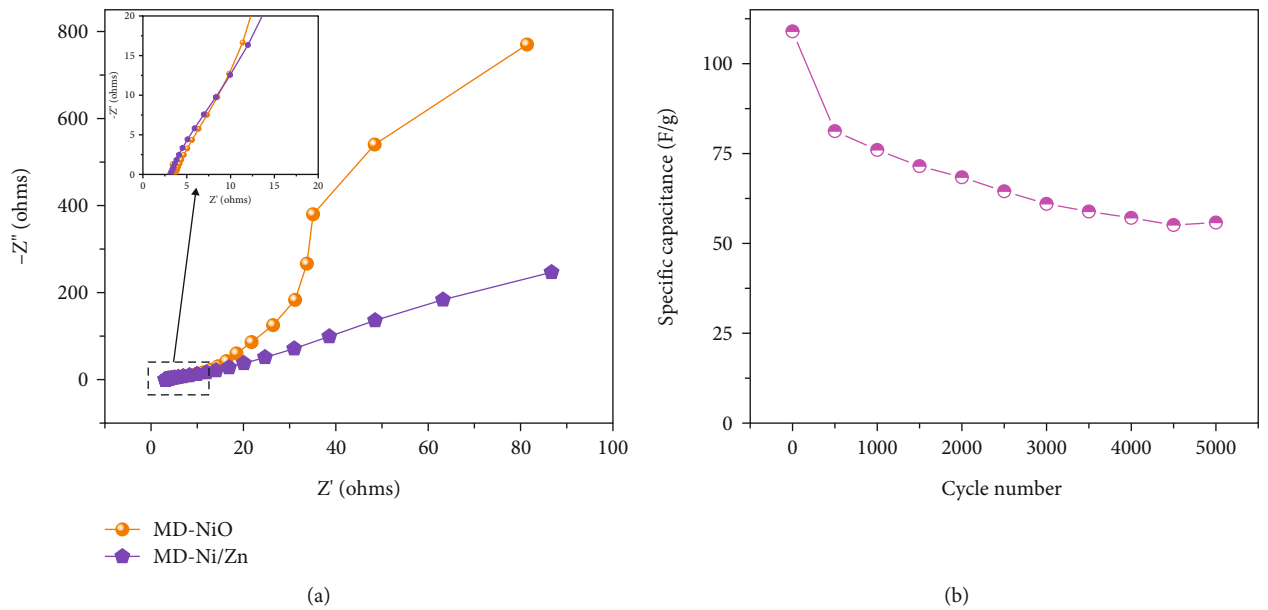

Figure 12: (a) EIS spectra of MD-NiO and MD-Ni/Zn composite electrodes and (b) cycling stability of MD-Ni/Zn composite electrodes.

rises within the range of 40.71-68.46%, while the diffusive contribution diminishes within the range of 59.28-31.53%. To gain a deeper understanding, we further analyzed the diffusion contribution to the total contribution by deconvolving the CV profile at a sweep rate of 5 mV/s, revealing a capacitive contribution of 60.56%. This finding underscores the role of K^+ ion intercalation within the electrode as a significant aspect of the electrochemical process (Figure 10(f)).

To comprehensively evaluate the charge storage capacity of the MD-Ni/Zn composite electrode, we conducted GCD analysis at several current densities (CD) within a 0-0.5 V potential range (Figures 11(a) and 11(b)). As the CD increased, the discharge time decreased, resulting in narrower plateaus in the discharge curves. This phenomenon is endorsed to the limited contact time between the electrolyte ions and the MD-Ni/Zn composite electrode, particularly noticeable at 10 A/g. A comparison of the GCD curves for MD-NiO and MD-Ni/Zn composite electrodes (Figure 11(c)) underscored the superior electrochemical storage capacity of the MD-Ni/Zn composite. Additionally, Figure 11(d) depicted the specific capacity of the MD-Ni/Zn composite at various CD, revealing capacitance values of 1002, 739, 323, and 110 F/g at 5, 6, 8, and 10 A/g, respectively. Notably, the specific capacitance decreased from 1002 to 110 F/g as from 5 to 10 A/g, consistent with typical electrochemical behavior. Table S1 offers an extensive analysis of the electrochemical attributes of the MD-Ni/Zn composite electrode in comparison to its MOF-based counterparts. The information contained within the table emphasizes the remarkable energy storage potential of the MD-Ni/Zn composite electrode.

In Figure 12(a), we present the EIS plots obtained for both MD-NiO and MD-Ni/Zn composite electrodes, and related equivalent circuit is presented in Figure S3. The slope of the EIS plot for the MD-Ni/Zn composite electrode exceeded 45°, indicating that the overall capacitance primarily results from ion diffusion [50]. In comparison to the diffusion-limited charge storage process observed in MD-NiO, the interior structure of the MD-Ni/Zn composite electrode appears to enhance the accessibility of OH^- ions to electroactive sites, resulting in a higher available capacitance [51]. The estimated solution resistance (R_s) values were determined to be 3.53 and 3.141 Ω, while the charge transfer resistance (R_{ct}) was found to be 28.56 and 6.71 Ω, with Warburg constants of 0.631 and 0.788 for MD-NiO and MD-Ni/Zn composite electrodes, respectively. This suggests improved ion mobility and higher electrochemical activity in the MD-Ni/Zn composite electrode, consistent with the observations mentioned earlier.

To assess electrode stability, cyclic performance tests were conducted at 10 A/g for 5000 cycles (Figure 12(b)). The MD-Ni/Zn composite electrode exhibited a capacitance retention of 51.1%. The initial drop in specific capacitance during the primary cycles is endorsed to the incomplete activation and utilization of the active material enclosed within the electrode. As electrochemical reactions progress, the internal electrode material progressively undertakes reactions, releasing energy and maintaining specific capacitance, followed by a gradual discharge-specific capacitance decline; this behavior aligns with previous reports [52]. Compared to the MD-NiO electrode, the MD-Ni/Zn composite electrode displays notable enhanced capacitance, which can be endorsed to the beneficial synergy effect of mixed oxide composite with their unique egg-yolk-like structure. This structure facilitates the penetration and transport of OH^- ions, contributing to the enhanced performance and stability of the composite electrode.

4. Conclusion

In this study, we investigated the photocatalytic and electrochemical characteristics of MOF-derived NiO-ZnO oxide

composites (MD-Ni/Zn). Our results revealed that the MD-Ni/Zn composite exhibited notable photocatalytic performance, degrading mixed dyes (RhB + CV) by 98% in 60 min under UV irradiation. The photocatalytic mechanism was elucidated, highlighting the type-II heterojunction between NiO and ZnO, which efficiently prevented the recombination of photoinduced e^-/h^+ pairs, leading to boosted photoactivity. Additionally, the MD-Ni/Zn composite electrode displayed notable electrochemical activity compared to MD-NiO, with a higher specific capacitance and redox activity. This enhancement was endorsed to the synergy effect of NiO and ZnO within the composite electrode. Furthermore, the MD-Ni/Zn electrode demonstrated admirable stability during cyclic performance tests, showcasing a retention efficiency of 51.1% after 5000 cycles. EIS analysis designated that the enhanced performance of MD-Ni/Zn was because of improved ion diffusion and lower charge transfer resistance. These findings suggest that the MD-Ni/Zn composite holds promise for applications in energy storage and wastewater treatment due to its exceptional electrochemical and photocatalytic properties.

Data Availability

All data are included in the manuscript.

Conflicts of Interest

The authors declare that they have no conflict of interest.

Authors' Contributions

JS and NDN were responsible for the conceptualization and writing of the original draft. SVPV was responsible for methodology and data acquisition. PR was responsible for data acquisition, writing, and revisioning. MRK and IAA were responsible for draft writing and editing. BK was responsible for conceptualization, writing, and editing.

Acknowledgments

The authors extend their appreciation to the Researchers Supporting Project number (RSPD2024R956), King Saud University, Riyadh, Saudi Arabia, and the National Research Foundation of Korea (number: RS-2023-00280665).

Supplementary Materials

Supplementary data: details of scavenger test, HRTEM images and EDX spectra, comparative analysis of optical absorbance spectra and Tauc plots, equivalent circuit, and comparison table showcasing the electrochemical activity of MD-Ni/Zn composite electrode with reports. *(Supplementary Materials)*

References

[1] Y. Zhang, J. Xu, J. Zhou, and L. Wang, "Metal-organic framework-derived multifunctional photocatalysts," *Chinese Journal of Catalysis*, vol. 43, no. 4, pp. 971–1000, 2022.

[2] P. Dhiman, G. Sharma, A. N. Alodhayb et al., "Constructing a visible-active $CoFe_2O_4$@Bi_2O_3/NiO nanoheterojunction as magnetically recoverable photocatalyst with boosted ofloxacin degradation efficiency," *Molecules*, vol. 27, no. 23, p. 8234, 2022.

[3] G. Rana, P. Dhiman, J. Sharma, A. Kumar, and G. Sharma, "Photocatalytic degradation of amoxicillin using TM doped ZnO nanoparticles synthesized from orange peel extract," *Inorganic Chemistry Communications*, vol. 158, article 111596, 2023.

[4] M. W. Alam, N. R. Khalid, S. Naeem et al., "Novel Nd-N/TiO2 nanoparticles for photocatalytic and antioxidant applications using hydrothermal approach," *Materials*, vol. 15, no. 19, p. 6658, 2022.

[5] P. Behera, S. Subudhi, S. P. Tripathy, and K. Parida, "MOF derived nano-materials: a recent progress in strategic fabrication, characterization and mechanistic insight towards divergent photocatalytic applications," *Coordination Chemistry Reviews*, vol. 456, article 214392, 2022.

[6] M. W. Alam, M. Aamir, M. Farhan et al., "Green synthesis of Ni-cu-Zn based nanosized metal oxides for photocatalytic and sensor applications," *Crystals*, vol. 11, no. 12, p. 1467, 2021.

[7] J. Sharma, P. Dhiman, A. Kumar, E. A. Dawi, G. Rana, and G. Sharma, "2D–2D g-C_3N_5/$Bi_{24}O_31Br_{10}$ S-scheme nanostructures with increased photocatalytic efficiency for crystal violet removal," *Chemical Engineering Research and Design*, vol. 195, pp. 432–446, 2023.

[8] D. Paul, S. Maiti, D. P. Sethi, and S. Neogi, "Bi-functional NiO-ZnO nanocomposite: synthesis, characterization, antibacterial and photo-assisted degradation study," *Advanced Powder Technology*, vol. 32, no. 1, pp. 131–143, 2021.

[9] H. Far, M. Hamici, N. Brihi et al., "High-performance photocatalytic degradation of NiO nanoparticles embedded on α-Fe_2O_3 nanoporous layers under visible light irradiation," *Journal of Materials Research and Technology*, vol. 19, pp. 1944–1960, 2022.

[10] J. Zeng, K. C. Devarayapalli, S. V. P. Vattikuti, and J. Shim, "Hierarchical 3D micro-nanostructures based on in situ deposited bimetallic metal-organic structures on carbon fabric for supercapacitor applications," *International Journal of Energy Research*, vol. 46, no. 5, pp. 6031–6044, 2022.

[11] W. Zhou, Y. Tang, X. Zhang, S. Zhang, H. Xue, and H. Pang, "MOF derived metal oxide composites and their applications in energy storage," *Coordination Chemistry Reviews*, vol. 477, article 214949, 2023.

[12] Y. Pan, S. Sanati, M. Nadafan, R. Abazari, J. Gao, and A. M. Kirillov, "Postsynthetic modification of NU-1000 for designing a polyoxometalate-containing nanocomposite with enhanced third-order nonlinear optical performance," *Inorganic Chemistry*, vol. 61, no. 47, pp. 18873–18882, 2022.

[13] S. Q. Zheng, S. S. Lim, C. Y. Foo et al., "A novel MOF-derived binary metal oxides and carbon nanocomposite for high-performance symmetric supercapacitor application," *Journal of Materials Science: Materials in Electronics*, vol. 34, no. 21, p. 1578, 2023.

[14] R. Das, S. S. Manna, B. Pathak, and C. M. Nagaraja, "Strategic design of Mg-centered porphyrin metal–organic framework for efficient visible light-promoted fixation of CO2 under ambient conditions: combined experimental and theoretical investigation," *ACS Applied Materials & Interfaces*, vol. 14, no. 29, pp. 33285–33296, 2022.

[15] T. Kalhorizadeh, B. Dahrazma, R. Zarghami, S. Mirzababaei, A. M. Kirillov, and R. Abazari, "Quick removal of

metronidazole from aqueous solutions using metal–organic frameworks," *New Journal of Chemistry*, vol. 46, no. 19, pp. 9440–9450, 2022.

[16] I. Hussain, S. Sahoo, T. Hussain et al., "Theoretical and experimental investigation of in situ grown MOF-derived oriented Zr-Mn-oxide and solution-free CuO as hybrid electrode for supercapacitors," *Advanced Functional Materials*, vol. 33, no. 7, p. 2210002, 2023.

[17] R. Abazari, S. Sanati, and A. Morsali, "Mixed metal Fe2Ni MIL-88B metal–organic frameworks decorated on reduced graphene oxide as a robust and highly efficient electrocatalyst for alkaline water oxidation," *Inorganic Chemistry*, vol. 61, no. 8, pp. 3396–3405, 2022.

[18] J. Xu, C. Xu, Y. Zhao, J. Wu, and J. Hu, "Hollow Co_3O_4@MnO_2 cubic derived from ZIF-67@Mn-ZIF as electrode materials for supercapacitors," *Frontiers in Chemistry*, vol. 7, p. 831, 2019.

[19] J. Wang, R. Abazari, S. Sanati et al., "Water-stable fluorous metal organic frameworks with open metal sites and amine groups for efficient urea electrocatalytic oxidation," *Small*, vol. 19, no. 43, 2023.

[20] L. Jin, X. Zhao, X. Qian, and M. Dong, "Nickel nanoparticles encapsulated in porous carbon and carbon nanotube hybrids from bimetallic metal-organic-frameworks for highly efficient adsorption of dyes," *Journal of Colloid and Interface Science*, vol. 509, pp. 245–253, 2018.

[21] Z. Li, X. Tang, G. Huang et al., "Bismuth MOFs based hierarchical Co_3O_4-Bi_2O_3 composite: an efficient heterogeneous peroxymonosulfate activator for azo dyes degradation," *Separation and Purification Technology*, vol. 242, article 116825, 2020.

[22] Y. Wang, X. Liu, L. Guo et al., "Metal organic framework-derived C-doped ZnO/TiO_2 nanocomposite catalysts for enhanced photodegradation of rhodamine B," *Journal of Colloid and Interface Science*, vol. 599, pp. 566–576, 2021.

[23] M. Wang, Y. Hu, J. Han, R. Guo, H. Xiong, and Y. Yin, "TiO2/NiO hybrid shells: p–n junction photocatalysts with enhanced activity under visible light," *Journal of Materials Chemistry A*, vol. 3, no. 41, pp. 20727–20735, 2015.

[24] W. Li, Z. Song, X. Deng, X. Fu, and J. Luo, "Decoration of NiO hollow spheres composed of stacked nanosheets with CeO2 nanoparticles: enhancement effect of CeO2 for electrocatalytic methanol oxidation," *Electrochimica Acta*, vol. 337, article 135684, 2020.

[25] M. W. Alam, A. BaQais, T. A. Mir, I. Nahvi, N. Zaidi, and A. Yasin, "Effect of Mo doping in NiO nanoparticles for structural modification and its efficiency for antioxidant, antibacterial applications," *Scientific Reports*, vol. 13, no. 1, p. 1328, 2023.

[26] Z. Zhang, C. Shao, X. Li, C. Wang, and M. Zhang, "Liu Electrospun nanofibers of p-type NiO/n-type ZnO heterojunctions with enhanced photocatalytic activity," *ACS Applied Materials & Interfaces*, vol. 2, no. 10, pp. 2915–2923, 2010.

[27] M. Wang, L. Sun, Z. Lin, J. Cai, K. Xie, and C. Lin, "Heterojunction photoelectrodes composed of Cu2O-loaded TiO2 nanotube arrays with enhanced photoelectrochemical and photoelectrocatalytic activities," *Energy & Environmental Science*, vol. 6, no. 4, pp. 1211–1220, 2013.

[28] P. Li, M. Zhang, X. Li et al., "MOF-derived NiO/CeO_2 heterojunction: a photocatalyst for degrading pollutants and hydrogen evolution," *Journal of Materials Science*, vol. 55, no. 33, pp. 15930–15944, 2020.

[29] X. Lei, Y. Cao, Q. Chen, X. Ao, Y. Fang, and B. Liu, "ZIF-8 derived hollow CuO/ZnO material for study of enhanced photocatalytic performance," *Colloids and Surfaces A: Physicochemical and Engineering Aspects*, vol. 568, pp. 1–10, 2019.

[30] S. Wu, J. Liu, H. Wang, and H. Yan, "A review of performance optimization of MOF-derived metal oxide as electrode materials for supercapacitors," *International Journal of Energy Research*, vol. 43, no. 2, pp. 697–716, 2019.

[31] K. Yang, Y. Yan, W. Chen et al., "Yolk-shell bimetallic metal-organic frameworks derived multilayer core-shells NiCo2O4/NiO structure spheres for high-performance supercapacitor," *Journal of Electroanalytical Chemistry*, vol. 851, article 113445, 2019.

[32] M. Aghazadeh and H. Foratirad, "Electrochemical grown Ni, Zn-MOF and its derived hydroxide as battery-type electrodes for supercapacitors," *Synthetic Metals*, vol. 285, article 117009, 2022.

[33] A. Tang, C. Wan, X. Hu, and X. Ju, "Metal-organic framework-derived Ni/ZnO nano-sponges with delicate surface vacancies as anode materials for high-performance supercapacitors," *Nano Research*, vol. 14, no. 11, pp. 4063–4072, 2021.

[34] F. Israr, D. Chun, Y. Kim, and D. K. Kim, "High yield synthesis of Ni-BTC metal-organic framework with ultrasonic irradiation: role of polar aprotic DMF solvent," *Ultrasonics Sonochemistry*, vol. 31, pp. 93–101, 2016.

[35] X. Zhang, Y. Sui, F. Wei et al., "Self-supported 3D layered zinc/nickel metal-organic framework with enhanced performance for supercapacitors," *Journal of Materials Science: Materials in Electronics*, vol. 30, pp. 18101–18110, 2019.

[36] D. R. Sun, F. X. Sun, X. Y. Deng, and Z. H. Li, "Mixed-metal strategy on metal-organic frameworks (MOFs) for functionalities expansion: Co substitution induces aerobic oxidation of cyclohexene over inactive Ni-MOF-74," *Inorganic Chemistry*, vol. 54, no. 17, pp. 8639–8643, 2015.

[37] C. K. Brozek and M. Dinca, "Ti3+-, V2+/3+-, Cr2+/3+-, Mn2+-, and Fe2+-substituted MOF-5 and redox reactivity in Cr- and FeMOF-5," *Journal of the American Chemical Society*, vol. 135, no. 34, pp. 12886–12891, 2013.

[38] T. T. Minh, N. T. T. Tu, T. T. V. Thi et al., "Synthesis of porous octahedral ZnO/CuO composites from Zn/Cu-based MOF-199 and their applications in visible-light-driven photocatalytic degradation of dyes," *Journal of Nanomaterials*, vol. 2019, Article ID 5198045, 16 pages, 2019.

[39] H. D. Weldekirstos, B. Habtewold, and D. M. Kabtamu, "Surfactant-assisted synthesis of NiO-ZnO and NiO-CuO nanocomposites for enhanced photocatalytic degradation of methylene blue under UV light irradiation," *Frontiers in Materials*, vol. 9, article 832439, 2022.

[40] T. Q. N. Tran, B. J. Park, W. H. Yun, T. N. Duong, and H. H. Yoon, "Metal–organic framework–derived Ni@C and NiO@C as anode catalysts for urea fuel cells," *Scientific Reports*, vol. 10, no. 1, p. 278, 2020.

[41] L. Ma, X. Ai, W. Jiang et al., "Zn/Ce metal-organic framework-derived ZnO@CeO_2 nano-heterojunction for enhanced photocatalytic activity," *Colloid and Interface Science Communications*, vol. 49, article 100636, 2022.

[42] J. Li, C. Zhang, Y. Wen et al., "Design of ZIF-67 MOF-derived Co3O4/NiCo2O4 nanosheets for supercapacitor electrode materials," *Journal of Chemical Research*, vol. 45, no. 11-12, pp. 983–991, 2021.

[43] L. Wei, D. Zeng, Z. Xie et al., "NiO nanosheets coupled with CdS nanorods as 2D/1D heterojunction for improved photocatalytic hydrogen evolution," *Frontiers in Chemistry*, vol. 9, p. 655583, 2021.

[44] L. Ma, X. Ai, Y. Chen et al., "Improved photocatalytic activity via n-type ZnO/p-type NiO heterojunctions," *Nanomaterials*, vol. 12, no. 20, p. 3665, 2022.

[45] L. Gnanasekaran, W. Chen, and M. Soto-Moscoso, "Highly operative NiO/ZnO nanocomposites for photocatalytic removal of azo dye," *Chemosphere*, vol. 308, Part 3, article 136528, 2022.

[46] S. Seenivasan, K. I. Shim, C. Lim et al., "Boosting pseudocapacitive behavior of supercapattery electrodes by incorporating a Schottky junction for ultrahigh energy density," *Nano Micro Letters*, vol. 15, no. 1, p. 62, 2023.

[47] P. Yang, X. Song, C. Jia, and H. S. Chen, "Metal-organic framework-derived hierarchical ZnO/NiO composites: morphology, microstructure and electrochemical performance," *Journal of Industrial and Engineering Chemistry*, vol. 62, pp. 250–257, 2018.

[48] S. V. P. Vattikuti, N. T. Hoai, J. Zeng, R. Ramaraghavulu, N. N. Dang, and C. M. Julien, "Pouch-type asymmetric supercapacitor based on Nickel–Cobalt Metal–Organic framework," *Materials*, vol. 16, no. 6, p. 2423, 2023.

[49] G. Li, P. Liu, R. Liu et al., "MOF-derived hierarchical double-shelled NiO/ZnO hollow spheres for high-performance supercapacitors," *Dalton Transactions*, vol. 45, no. 34, pp. 13311–13316, 2016.

[50] S. Q. Zheng, S. S. Lim, C. Y. Foo et al., "Solvothermal synthesis of nanostructured nickel-based metal–organic frameworks (Ni-MOFs) with enhanced electrochemical performance for symmetric supercapacitors," *Journal of Materials Science*, vol. 58, no. 29, pp. 11894–11913, 2023.

[51] S. Ebrahimi-Koodehi, F. E. Ghodsi, and J. Mazloom, "Mixed metallic NiFe/Mn-MOF, and derived spinel Ni0.5Fe0.5Mn2O4 as high-performance electrochemical electrodes," *International Journal of Energy Research*, vol. 46, no. 15, pp. 24368–24380, 2022.

[52] S. Arshadi Rastabi, R. Sarraf-Mamoory, G. Razaz, N. Blomquist, M. Hummelgård, and H. Olin, "Treatment of $NiMoO_4$/nanographite nanocomposite electrodes using flexible graphite substrate for aqueous hybrid supercapacitors," *PLoS ONE*, vol. 16, no. 7, article e0254023, 2021.